Solar Energy Materials & Solar Cells 293 (2025) 113854

Contents lists available at ScienceDirect

Solar Energy Materials and Solar Cells

journal homepage: www.elsevier.com/locate/solmat

Light and elevated temperature induced degradation in gallium-doped silicon: A complete parametric description

Fabian T. Thome [a,*], Elvin Garashli [a], Wolfram Kwapil [a,b], Florian Schindler [a], Martin C. Schubert [a]

[a] Fraunhofer Institute for Solar Energy Systems (ISE), Heidenhofstr. 2, Freiburg im Breisgau, 79110, Germany
[b] Department of Sustainable Systems Engineering (INATECH), Emmy-Noether-Straße 2, Freiburg im Breisgau, 79110, Germany

ARTICLE INFO

Keywords:
Gallium-doped
Light and elevated temperature induced degradation (LeTID)
Silicon
p-type
Photovoltaics
Temporary recovery

ABSTRACT

Despite extensive research on light and elevated temperature induced degradation (LeTID), a complete quantitative description of all relevant subprocesses is still lacking. In particular, the phenomenon of temporary recovery, which opposes the degradation transition, is poorly understood. In this study, we treat gallium-doped Czochralski silicon wafers at varying temperatures and minority charge carrier densities, measuring the resulting changes in effective lifetime. By studying temporary recovery in isolation from degradation and regeneration, we find that the rate of temporary recovery increases as temperature decreases. This is quantified by a negative activation energy of $E_a^{BA} = -0.6$ eV. This *reversed* Arrhenius behavior imposes restrictions on the reaction scheme, suggesting that temporary recovery is a multi-step process involving at least two distinct subreactions. The dependence of temporary recovery on the minority charge carrier density was found to follow a power law with an exponent around $x_{BA} = 1.9$. For degradation and regeneration, we derive activation energies close to 0.8 eV. This similarity of the temperature dependence is consistent with a recently proposed atomistic model, where both degradation and regeneration occur by atomic hydrogen binding to another complex.

In total, we have provided all kinetic parameters required for describing LeTID in gallium-doped silicon with the well-known three-state model. Our findings thereby not only enhance the understanding of the underlying processes involved in LeTID, but also enable the precise modelling of the degradation rate and extent. These results lay the groundwork for complex outdoor yield models that incorporate weather data.

1. Introduction

Silicon photovoltaics continue to dominate the market, benefiting from a long history of scientific research and cost reduction [1,2]. Despite the technology's maturity, the pursuit of profit optimization still drives substantial innovation along the whole production chain [3,4]. A prominent example is the rapid transition of the wafer dopant atom from boron to gallium to phosphorus and most recently to antimony [1,5]. While such technological flexibility supports the growth of photovoltaics, it also poses a significant challenge for reliable long-term stability assessment.

The progression of light and elevated temperature induced degradation (LeTID) is severely influenced by the choice of dopant atom [6]. LeTID was first studied in boron-doped silicon [7–10], but has since been shown to occur for gallium- [6,11–14], phosphorus- [15,16] and antimony- [17] doped material as well. A typical LeTID sequence consists of the transformation of precursors into bulk defects followed by a much slower regeneration process [18,19]. Unlike precursors, regenerated species are stable against temperature and light stress encountered during field application [20]. Hammann et al. recently proposed an atomistic model for LeTID built on measurements and simulations in boron-doped silicon [21,22]. The precursors are therein associated with the complex XH_2 consisting of an unidentified species X and hydrogen molecules. Degradation and regeneration consecutively occur by atomic hydrogen bonding to the complex, i.e. the reactions $XH_2 + H \rightarrow XH_3$ and $XH_3 + H \rightarrow XH_4$, respectively. Studies on boron- and gallium-doped silicon were able to link the hydrogen molecule concentration directly to the LeTID extent, which initiated the hypothesis that LeTID-precursors consist in parts of hydrogen molecules [22,23]. This also explains why processing techniques that reduce the hydrogen molecule concentration

This article is part of a special issue entitled: SiliconPV 2025 published in Solar Energy Materials and Solar Cells.

* Corresponding author. Fabian Thome, Heidenhofstr. 2, 79110, Freiburg im Breisgau, Germany.
E-mail address: fabian.thome@ise.fraunhofer.de (F.T. Thome).

https://doi.org/10.1016/j.solmat.2025.113854
Received 13 June 2025; Received in revised form 10 July 2025; Accepted 17 July 2025
Available online 26 July 2025

in the bulk can help to mitigate the degradation extent [24–27]. The relevant parameters determining the precursor concentration are the firing temperature and cooling ramp [24,26,28–31], the wafer thickness [25,32] and the passivation stack [27,33–37].

The main difference between gallium- and boron-doped silicon is the rate and extent of degradation. Gallium-doped material is associated with a slower progression and a lower degradation extent [6,12,38–40]. The enhanced LeTID-resilience is attributed to the backward transition from defect to precursor being more dominant when gallium is used as a dopant atom [41]. This transition, termed temporary recovery, can be dominant in gallium-doped silicon for the whole temperature range expected in the field [38,41]. The inherent tendency towards temporary recovery, combined with the effective mitigation strategies, likely accounts for the exceptional stability of industrial gallium-doped solar cells against LeTID [42,43]. However, research on temporary recovery is still scarce [38,41], and both an atomistic interpretation and a comprehensive kinetic description are lacking.

We systematically investigate temporary recovery, degradation and regeneration in gallium-doped silicon as functions of temperature and minority charge carrier density. Our findings reveal a reversed Arrhenius behavior for temporary recovery, suggesting a composite reaction on the atomic level. Using the extracted kinetic parameters, we can precisely model the rate and extent of LeTID in gallium-doped silicon.

2. Theory

The theoretical framework used for the description of LeTID is the three-state model depicted in Fig. 1. It assumes that the populations of the precursors (state A), defects (state B) and regenerated species (state C) are determined by the first order reactions degradation (A→ B), regeneration (B→C) and temporary recovery (B→A). Transitions that could appear at higher temperatures than probed in this paper (140 °C), for example the replenishment of precursors from a reservoir state [19], are not incorporated.

The differential equations for the state populations are:

$$\frac{dA(t)}{dt} = -k_{AB}A(t) + k_{BA}B(t) \tag{1}$$

$$\frac{dB(t)}{dt} = k_{AB}A(t) - k_{BA}B(t) - k_{BC}B(t) \tag{2}$$

$$\frac{dC(t)}{dt} = k_{BC}B(t) \tag{3}$$

The transitions between states are characterized by their rate coefficients k_{ij} with $i,j \in \{A,B,C\}$ and $i \neq j$ that incorporate the system's dependence on temperature T and minority charge carrier density Δn:

$$k_{ij}(T,\Delta n) = \nu_0 \left(\frac{\Delta n}{\Delta n_0}\right)^{x_{ij}} \exp\left(-\frac{E_a^{ij}}{k_B T}\right) \tag{4}$$

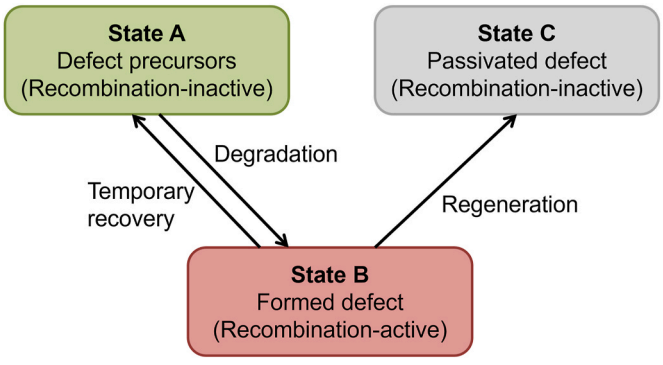

Fig. 1. Sketch of the LeTID-states and the transitions that are dominant at and below 140 °C. Adapted from Ref. [38].

Here, ν_0 denotes a preexponential factor, the injection exponent x_{ij} is often interpreted as the stoichiometric factor in a minority charge carrier-driven reaction, $\Delta n_0 = 1\text{cm}^{-3}$ is introduced for normalization and the activation energy E_a^{ij} as well as the Boltzmann constant k_B appear in the characteristic Arrhenius-law.

So far, there is no method to measure the concentration of species in states A and C. However, the normalized defect density NDD(t) can reflect changes of the defect state population B(t) with respect to a reference point:

$$NDD(t) = \frac{1}{\tau(t)} - \frac{1}{\tau_{ref}} \propto B(t) - B_{ref} \tag{5}$$

This proportionality is strictly valid only if a single type of defect is created throughout the treatment time t. It should thus be kept in mind that the introduction or curing of non-LeTID type defects can affect the NDD based analysis.

Describing NDD data with the full three-state model can lead to overfitting. It is thus advisable to investigate limiting cases where some transitions can be neglected. In the case where temporary recovery is the only active process ($k_{AB} \approx k_{BC} \approx 0$), the three-state-model predicts a monoexponential decay of the preexisting defect population B_0:

$$NDD(t) \propto B(t) - B_{ref} = B_0 \exp(-k_{BA}t) - B_{ref} \tag{6}$$

If an initially defect free ($B_0 = 0$) sample undergoes pure degradation and regeneration, i.e. $k_{BA} \approx 0$, the evolution of LeTID defects B(t) is given by:

$$NDD(t) \propto B(t) = \frac{k_{AB}A_0}{k_{AB} - k_{BC}} (\exp(-k_{BC}t) - \exp(-k_{AB}t)) \tag{7}$$

where the parameter A_0 denotes the precursor population A(t) at t = 0 and $B_{ref} = 0$ was assumed. A more detailed discussion on the three-state model and the challenges connected to extracting transition coefficients from measurements of NDD curves can be found in Ref. [41].

3. Experimental details

Two groups of gallium-doped silicon wafers symmetrically passivated with silicon nitride were studied in this work. The wafers of group 1 (0.84 Ωcm) were used for the experiments investigating degradation and regeneration (section 4.2). The wafers of group 2 (0.84 Ωcm) used for investigating temporary recovery (section 4.1) stem from the same manufacturer but were processed several months later. The measured peak firing temperature had to be reduced from $T_{group\ 1} = 800°C$ to $T_{group\ 2} = 760°C$ to obtain satisfying effective lifetimes. Otherwise, the processing was exactly equal and is described in detail in Ref. [41].

To reliably obtain the rate coefficients k_{ij} from fits to NDD curves, both temperature and injection must be held constant throughout the treatment. For a constant injection, any change of the effective lifetime must be accounted for by an adaptation of the charge carrier generation ($\Delta n = G \cdot \tau$). For the experiments tracking degradation and regeneration (section 4.2), the samples were placed on precision hot plates (Präzitherm) and under LED lamps. This setup was also used to prepare LeTID defects for the experiments focusing on temporary recovery (section 4.1). The effective lifetime was measured ex-situ with a WCT-120TS Sinton Instruments lifetime tester. The scheme of iterative regulation that enabled a treatment at constant injection is described in Ref. [41].

For the experiments described in section 4.1, the Modulum setup [44] was used to drive temporary recovery at the specified conditions while also measuring calibrated photoluminescence (PL)-images and modulated PL. The setup's chuck is water-cooled to 25 °C and can be regulated via Peltier elements for temperatures other than 25 °C. An 808 nm laser was used to illuminate the sample while taking PL-images. Using the concept of calibrated PL-imaging [44,45], the spatially

resolved effective lifetime and minority charge carrier density images were obtained. The laser power was automatically adapted such that the median of the minority charge carrier density in the homogeneous center area remained constant throughout the treatment. This automated in-situ approach assured that the injection stays within 5% of the targeted value even when the effective lifetime changes rapidly (see Supplementary Fig. S1a and S1b). The almost continuous laser illumination inadvertently heats the sample, causing a systematic increase from the target temperature. This effect is most dominant at the highest injection ($6 \times 10^{15}\mathrm{cm}^{-3}$), which relates to laser illumination with an intensity between 1 and 1.5 suns equivalent. However, the absolute temperature increase remains below 3 °C for a continuous illumination with 1.5 suns equivalent.

The in-situ characterization via calibrated PL images has the drawback that the lifetime is evaluated at the minority charge carrier density at which the sample is treated. Due to the injection dependent recombination activity of the LeTID defect, the measured absolute values of NDD depend strongly on the injection at which the lifetime is evaluated. This does not affect the kinetics or the extraction of kinetic parameters (see Supplementary Fig. S2). Non-spatially resolved modulated PL was used complementary since it offers injection dependent information of the effective lifetime [46–48]. However, modulated PL exposes the sample to a varying laser intensity, thereby driving temporary recovery forward in an unaccounted manner. This effect was only negligible for the highest injection setting $\Delta n = 6 \times 10^{15}\mathrm{cm}^{-3}$ used in this paper, forcing us to rely only on PL imaging for the remaining ones. In the following, the figure caption will always explain whether the data is based on calibrated PL-imaging or modulated PL.

4. Results

The transitions governing LeTID are best investigated in an isolated manner. We thus first focus on the low temperature regime, where temporary recovery shifts the population from the defect state to the precursor state. The processes degradation and regeneration, that drive the LeTID-cycle from state A via B to state C, are studied in section 4.2. Finally, section 4.3 merges the obtained results within the framework of the full three-state model.

4.1. On temporary recovery

4.1.1. Variation of temperature

As a pre-treatment, the group 2 samples were first treated at 25 °C and $\Delta n = 6 \times 15\,\mathrm{cm}^{-3}$ until the effective lifetime saturated. This can recover potential defects present in the as-fired state. The lifetime at the end of this step is used as the reference point for NDD calculations since it is closest to a fully defect free state. Afterwards, the samples were degraded at 120 °C and 1 sun equivalent illumination at the LED setup for 24 min. This duration was selected to create a significant defect population B_0 while not yet regenerating the sample. In the subsequent main experiment, each sample was treated at a fixed injection ($\Delta n = 6 \times 10^{15}\mathrm{cm}^{-3}$) and temperature (ranging from 25 °C to 60 °C) until the effective lifetime plateaued. Using temperatures below 60 °C ensures that degradation and regeneration transitions have little to no impact [38,41]. We prove that the transitions between states A and B are reversible by cycling a sample ten times between recovered and partially degraded state. Notably, neither the recovered NDD nor the transition coefficient of temporary recovery depend on the cycle number (see Supplementary Fig. S3a and S3b).

During the main experiment, the effective lifetime increases to the level it had prior to the degradation step, again suggesting full reversibility of the degradation. This is reflected in the decay in NDD down to zero as shown in Fig. 2. The slightly negative NDD values seen for the samples treated at 30 °C and 60 °C are likely due to healing of other defects unrelated to LeTID [49–51]. The systematic difference caused by

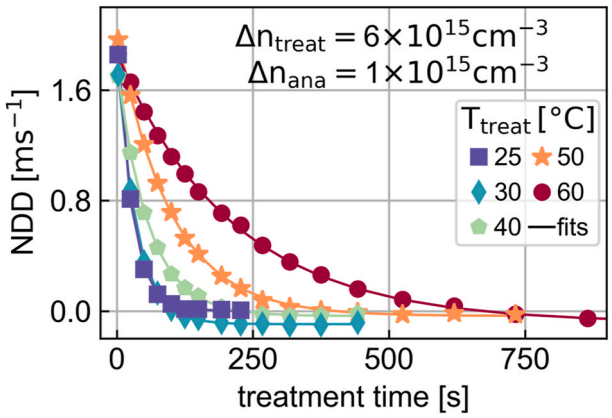

Fig. 2. Temporary recovery decreases the normalized defect density over time. Measured during the main experiment using modulated PL, analyzed at $\Delta n_{ana} = 10^{15}\mathrm{cm}^{-3}$. The lines are fits to equation (6).

the temperature variation lies in the rate of NDD decay, which increases for decreasing temperatures. This shows that temporary recovery, which is responsible for the observed reduction of NDD, occurs faster as the temperature is reduced.

To obtain quantitative information on temporary recovery, we extract the rate coefficients k_{BA} by fitting equation (6) to the NDD curves. The perfect alignment between fits and data showcases the validity of reducing the full three-state model to a purely temporary recovery dominated process at the tested temperatures. To complement the data in Fig. 2, two more temperature variations at different injections were added. Fig. 3 shows the temperature dependence of the corresponding transition coefficients k_{BA} in an Arrhenius representation. Fitting the transition coefficients to equation (4) leads to negative activation energies for all injection conditions (see inset of Fig. 3) that average to a value of $E_a^{BA} = -0.6\mathrm{eV}$.

Notably, the activation energy appears to become more negative with decreasing injection. The origin of this behavior could be twofold. On the one hand, the systematic deviation between targeted and actual temperature caused by the continuous laser illumination can lead to an underestimation of the absolute value of the activation energy, which would be most dominant at high injections. However, the offset by 2 °C is far too weak to explain the variation in activation energy. On the other hand, the decoupling of temperature and injection dependence as

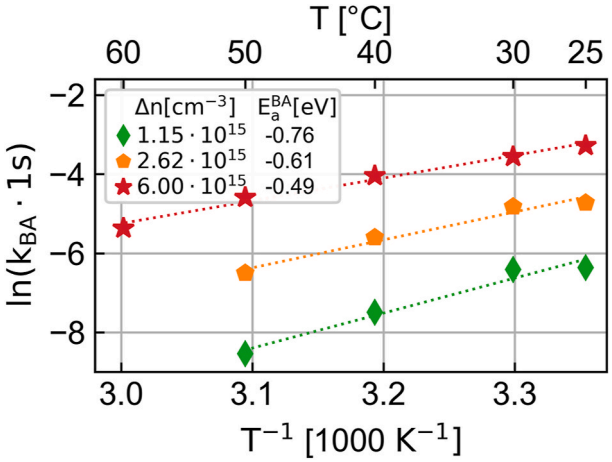

Fig. 3. The transition coefficients k_{BA} associated with temporary recovery show a reversed Arrhenius behavior with a negative activation energy.

assumed in equation (4) could be unrepresentative of the underlying physical mechanisms. The presence of charge carriers can certainly alter the configurational space of a reaction and thereby affect the measurable activation energy [52]. In our case, a weak, possibly logarithmic dependence of the activation energy on the minority charge carrier density is observed (see Supplementary Fig. S4). However, the data is inconclusive, since the uncertainties in the setup's temperature are too large.

In other literature, the temperature dependence of temporary recovery has so far only been described quantitatively in a single publication for multicrystalline boron-doped PERC cells [38]. Here, the rate coefficients for temporary recovery also showed a reversed Arrhenius behavior but the value for the activation energy was not extracted due to large experimental uncertainties. Revisiting the data of reference [38] yields an activation energy for temporary recovery in boron-doped silicon of (-0.40 ± 0.14) eV. The temperature dependence in boron- and gallium-doped silicon thus seems to be qualitatively similar, although the large uncertainty impedes a quantitative comparison. The qualitative similarity appears to contrast with our previous findings, where we showed that temporary recovery suppresses LeTID in gallium-doped silicon at conditions where it is negligible in boron-doped silicon [41]. However, even a small difference in activation energy can have a large impact on the rate equilibria due to the exponential Boltzmann factor. Furthermore, the preexponential factor is not known for boron-doped silicon, but could also explain the weaker impact of temporary recovery when compared to gallium-doped silicon.

The finding of a reversed Arrhenius behavior is most likely also valid for p-type silicon solar cells and modules. This is evident from outdoor module monitoring which showed an excessive LeTID-recovery during winter periods [53–55]. A negative activation energy is required to model this recovery [56]. Overall, the indications from the literature and the clarity of the reversed Arrhenius behavior of our data strongly suggest that the observed negative activation energy is reasonable.

A physical explanation for a negative activation energy can be found by consulting a chemistry textbook such as reference [57]. A direct reaction, as shown in Fig. 4a, leads to a positive activation energy. Its value corresponds to the largest energy difference along a reaction coordinate between the start state S and final state F. There are, however, plenty of processes where negative activation energies are observed [58–60], the most prominent being a subreaction in the ozone depletion cycle [61]. In these cases, a composite reaction

$$S \underset{k_1'}{\overset{k_1}{\rightleftarrows}} I \xrightarrow{k_2} F \tag{8}$$

via an intermediate state I is required (Fig. 4b). The second forward transition I → F must be rate limiting such that $k_1' \gg k_2$. This means that intermediate species tend to return to the start state rather than continuing to the final state. Such a system will assume a quasi-equilibrium between states S and I characterized by the equilibrium constant K:

$$K = \frac{I}{S} = \frac{k_1}{k_1'} \tag{9}$$

The rate of change in the final state

$$\frac{dF}{dt} = k_2 I = \frac{k_2 k_1}{k_1'} S = k_c S \tag{10}$$

is then governed by a composite reaction coefficient k_c

$$k_c = \frac{k_2 k_1}{k_1'} = \frac{A_2 A_1}{A_1'} \exp\left(-\frac{E_1 + E_2 - E_1'}{k_B T}\right) \tag{11}$$

Here, it was assumed that all subreactions follow the Arrhenius law $k_i = A_i \exp\left(-\frac{E_i}{k_B T}\right)$ where each individual activation energy E_i is positive. The composite reaction then has an apparent negative activation energy if

$$E_1' > (E_1 + E_2) \tag{12}$$

This quantitative argument can also be understood more intuitively. The backward transition I→S delays populating the final state and thereby decelerates the overall reaction. If the temperature dependence of the backward transition is stronger than that of the forward transitions, an increase in temperature effectively strengthens this braking force in the reaction. As a result, the full reaction will occur slower at higher temperatures. At much lower temperatures ($k_B T \ll E_2$), the reverse transition would ultimately be freezed out. This limits the range where the backward transition I→S is relevant and a reversed Arrhenius behavior is observable (see Supplementary Fig. S5). The onset of such a freeze out could possibly explain the slight deviation from the Arrhenius behavior observed for the points at 25 °C in Fig. 3.

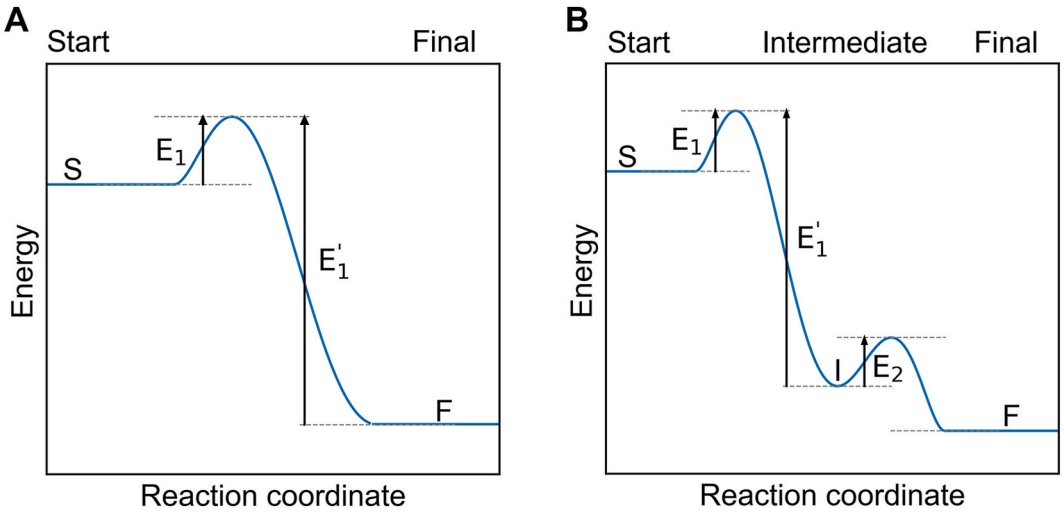

Fig. 4. A direct reaction (a, left) between start and final state cannot explain a negative activation energy. With an intermediate state (b, right) however, a composite reaction coefficient can feature a negative activation energy if $E_1' > E_1 + E_2$.

We speculate that the reactions underlying temporary recovery are of similar nature as described here. The defect state B is then equivalent with the start state S while the precursor state A is identified with the final state F. The experimentally determined transition coefficients k_{BA} would then be the composite reaction coefficients of a two-step reaction. Unfortunately, the measured monoexponential decay in NDD does not hold sufficient information to extract the individual rate coefficients k_1, k_1' and k_2.

Assuming the mechanisms' validity, we can nonetheless find constraints for the parameters such that the Arrhenius behavior is upheld. The first is that the activation energies must fulfill equation (12). This also implies that $E_1' > E_2$. Since the second forward transition must be rate limiting ($k_2 \ll k_1'$), the associated preexponential factor must be much smaller than that of the backward transitions, i.e. $A_1' \gg A_2$.

For a physical interpretation of this last constraint ($A_1' \gg A_2$), the simplification of the configuration space to a one-dimensional reaction coordinate (Fig. 4) must be relaxed to a two-dimensional view. Here, minima become saddle points, whose broadness (in addition to their height) also determines the likelihood of a transition. A particularly narrow saddle point reduces the number of probable reaction pathways and therewith the associated reaction rate. If the saddle point between I and S is broad while that between S and F is narrow, A_1' would be much larger than A_2. The rate limiting behavior of k_2 can thus be explained by an entropic argument [62].

For the application to LeTID in the framework of the three-state model, it should be noted that the preexponential factors are not equivalent to attempt frequencies as they likely incorporate concentration dependencies of other reactants, in particular the dependence on the minority charge carrier density Δn. This offers a pathway of investigation, since a variation in minority charge carrier density could then also impact the ratio of preexponential factors. Another approach to probe the behavior of temporary recovery could be to further reduce the temperature and try to freeze out the backward transition. However, our setup does not allow precise control of temperature below the tested conditions. As a final note, we would like to stress that it is unclear whether the hypothesized intermediate state in temporary recovery is recombination active or inactive. This is because its population can be insignificantly low with respect to the start and final states while still causing the reversed Arrhenius behavior.

4.1.2. Variation of minority charge carrier density

In the experiment focusing on the effects of minority charge carrier density on temporary recovery, LeTID defects were prepared using the same pre-treatment as described in section 4.1.1. The main experiment then consisted of their recovery at 25 °C and Δn_{treat} ranging from 0.5×10^{15} to $6 \times 10^{15} cm^{-3}$. Note that the minority charge carrier density is held constant for each individual run.

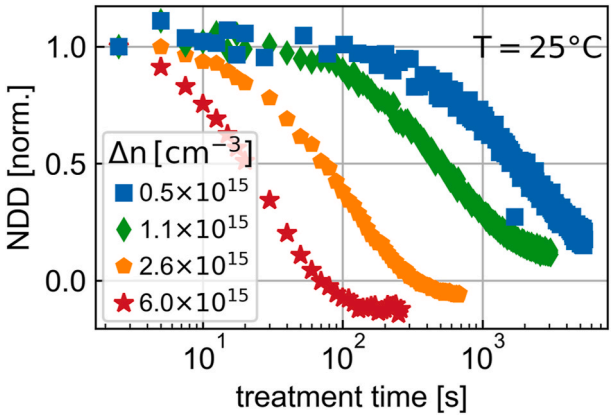

Fig. 5. Temporary recovery decreases the NDD (normalized) over time. Measured during the main experiment using calibrated PL imaging. For the non-normalized version, see Supplementary Fig. S6.

Fig. 5 shows the decay of NDD due to temporary recovery over the course of the main experiment. It is apparent that a higher minority charge carrier density accelerates the rate at which defects are recovered. For low injection conditions, impractically long experiment durations forced us to stop the experiment before a full saturation was achieved. Nevertheless, the extrapolation of the data suggests that a full recovery is in principle possible in all cases. This suggests that temporary recovery is the only dominant LeTID transition at the tested condition, since a finite defect density would remain if degradation was significant [41]. In some cases, the NDD reduces to values slightly below zero. This indicates that the sample had defects at the time of the reference measurement (after the first part of the pre-treatment) that were healed during the main experiment (compare equation (5)). Overall, the minority charge carrier density accelerates temporary recovery but does not appear to alter the behavior qualitatively.

To complement the data in Fig. 5, one more injection variation at 40 °C was added. With equation (6), the transition coefficients k_{BA} for the full dataset were obtained. The variation of minority charge carrier density allows to extract the injection exponents as the slopes from Fig. 6. This assumes the validity of equation (4) and thereby neglects any injection dependence of the activation energy. The values of 25 °C and 40 °C average to $x_{BA} = 1.9$. This value is similar to the report by Kwapil et al. for multicrystalline boron-doped material [38] and our previous results on gallium-doped material [41]. Since the value lies close to an integer number, it appears reasonable that the injection exponent represents a stoichiometric factor in the underlying chemical reaction. With the newly obtained image of temporary recovery as a composite reaction, several possibilities arise. To name just one option, the injection dependence of the transition coefficients k_1 and k_1' could cancel, while the second forward reaction might require two electrons ($k_2 \propto \Delta n^2$) and thus $k_c \propto \Delta n^2$ (compare equation (11)).

4.2. On degradation and regeneration

We investigated the kinetics of degradation and regeneration with samples of group 1 by treating them at $\Delta n = 1.34 \times 10^{15} cm^{-3}$ and temperatures varying from 100 °C to 140 °C, where only degradation and regeneration are dominant [41].

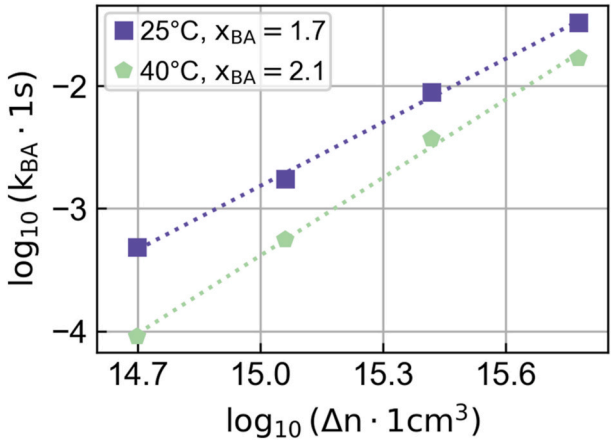

Fig. 6. The transition coefficients k_{BA} associated with temporary recovery shown as a function of the minority charge carrier density. The slope of the figure yields the injection exponents for 25 °C and 40 °C which are crucial for yield modelling.

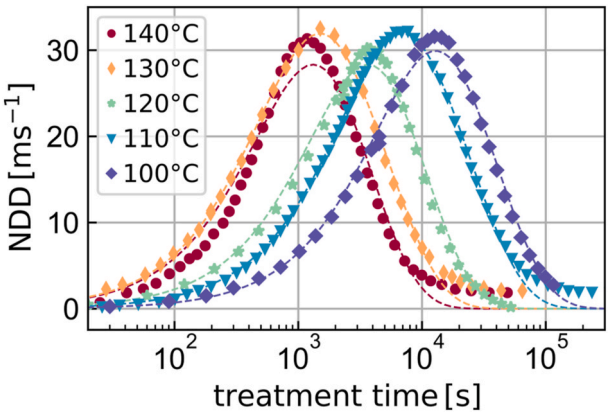

Fig. 7. The NDD as a function of treatment time during a typical LeTID cycle consisting of degradation and regeneration at $\Delta n_{treat} = 1.34 \times 10^{15} cm^{-3}$. The NDD is calculated based on lifetime measurements taken with a Sinton lifetime tester evaluated at $\Delta n_{ana} = 10^{15} cm^{-3}$. The dashed lines are fits to equation (7).

Fig. 7 shows the NDD for the full LeTID cycle. We find that increasing the temperature accelerates the LeTID cycle without significantly affecting the degradation extent. A fit of equation (7) to the NDD curves results in the transition coefficients of k_{AB} and k_{BC} as a function of temperature. We use a global fit to determine one value for the precursor density $A_0 = 43\ ms^{-1}$ for all samples. This approach is described in detail in Ref. [41].

The transition coefficients are shown in an Arrhenius representation in Fig. 8. The agreement with the Arrhenius law is evident for both transitions. It appears the two processes share a similar temperature dependence. This is also seen in the fit of equation (4) yielding activation energies of $E_a^{AB} = 0.79 \pm 0.11$ eV and $E_a^{BC} = 0.85 \pm 0.06$ eV that are identical within their error bounds. The similarity in the activation energies suggests that the underlying physical reaction could be similar too. This would be consistent with the LeTID reaction model suggested recently by Hamman et al. [21,22] where both degradation and regeneration are associated with atomic hydrogen bonding to a preexisting complex.

The value for E_a^{AB} is in line with our previous results as well as other literature that investigates the kinetics of LeTID in gallium-doped silicon at constant injection [23,41]. For regeneration in gallium-doped silicon, we are the first to have extracted a reliable value for the activation energy at constant minority charge carrier density and can therefore not compare with existing literature.

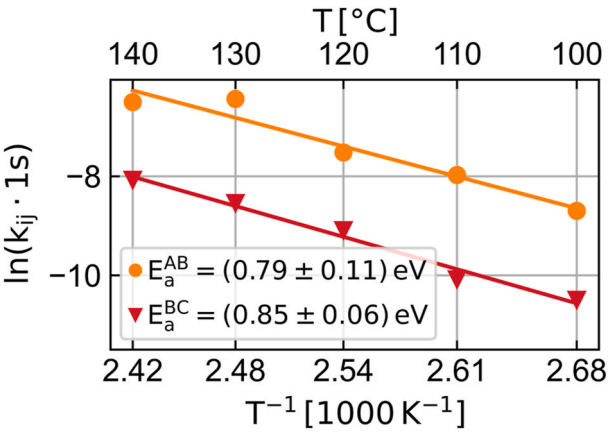

Fig. 8. Transition coefficients for degradation (orange circles) and regeneration (red triangles) as a function of inverse temperature. Both transitions follow an Arrhenius law allowing the extraction of the activation energy from the slope of the plot. The injection was held constant at $\Delta n_{treat} = 1.34 \times 10^{15} cm^{-3}$. (For interpretation of the references to color in this figure legend, the reader is referred to the Web version of this article.)

Table 1
Proposed kinetic parameters for the description of LeTID in gallium-doped silicon. These parameters enable the calculation of the transition coefficients via equation (4). In combination with equations (1)–(3), the progression of LeTID can be modelled.

Transition	Activation energy [eV]	Injection exponent	Preexponential factor ν_0 [1/s]
Degradation	0.79	1	6.2×10^{-9}
Regeneration	0.85	1	5.6×10^{-9}
Temporary recovery	−0.6	1.9	2.8×10^{-42}

4.3. On the three-state model

With reference [41] and this contribution, we have gathered a complete set of kinetic parameters for the phenomenological description of LeTID in Si:Ga. The results are summarized in Table 1. The pre-exponential factors are determined from a fit of equation (4) to the available transition coefficients with the activation energy and injection exponent fixed.

Inserting these kinetic parameters into equation (4) allows to calculate the transition coefficients for degradation, regeneration and temporary recovery as a function of both temperature and minority charge carrier density. With the differential equations of the three state model (equations (1)–(3)), the population of precursors, defects and regenerated species can be numerically integrated over time given any initial configuration. This approach is not restricted to constant temperatures or minority charge carrier densities. Instead, it can also incorporate variable conditions, for example gathered from outdoor weather data.

We now utilize the full description of LeTID in gallium-doped silicon to illustrate some of its properties. Of primary interest is the degradation extent. It was shown that the degradation extent is significantly influenced by the hydrogen molecule concentration in the specimen [23]. In terms of the three-state model, the hydrogen concentration thus determines the precursor density A_0. However, a full LeTID cycle never converts the full precursor density into recombination-active LeTID defects. The maximum degradation extent rather also depends on the treatment conditions.

This is shown in Fig. 9, where the maximum degradation extent is color-coded and plotted in the 2d-parameter space consisting of temperature and injection. At very high temperatures, a plateau of almost

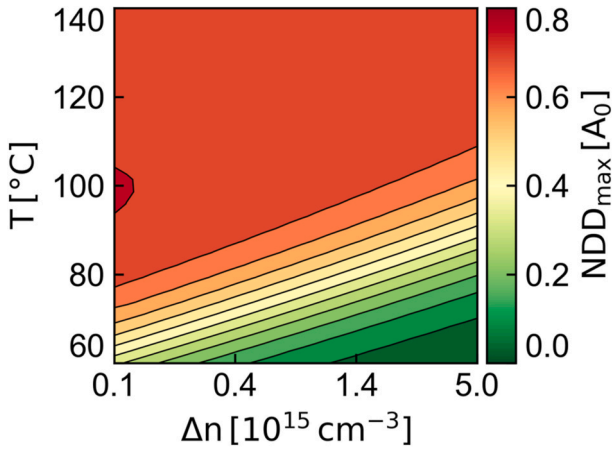

Fig. 9. Maximum degradation extent in proportion to the precursor density as a function of temperature and injection. At high temperatures and low injection, degradation and regeneration dominate the kinetics, giving similar degradation extent over the large red plateau. Towards the bottom right, temporary recovery sets in and suppresses LeTID. (For interpretation of the references to color in this figure legend, the reader is referred to the Web version of this article.)

equal degradation extent is observed. A strong gradient sets in towards lower temperatures and higher injections, leading to a continuous suppression of LeTID even at finite precursor density. To illustrate why these transitions occur, it is helpful to inspect the deviation between the full model and a simplified case where temporary recovery is neglected:

$$\sigma_{NDD}(k_{BA}=0)=\frac{\left|NDD_{max}^{full}-NDD_{max}^{k_{BA}=0}\right|}{NDD_{max}^{k_{BA}=0}} \quad (13)$$

In Fig. 10, the deviation between the full model and that neglecting temporary recovery is shown. Temporary recovery is evidently negligible for high temperatures (white region). This means the kinetics are only determined by degradation and regeneration. Since these two processes share similar kinetic parameters, the degradation extent does not vary over a large range of temperatures and injection values creating the plateau of Fig. 9 [41]. The value of the plateau is at around 70 % of the initial precursor population A_0. Physically, the regeneration process depletes the defect concentration before it can reach the initial precursor level. The range where regeneration has a major impact (more than 15 %) on the degradation extent is mostly confined to this plateau and thereby to temperatures exceeding field application values (see Supplementary Fig. S7).

When moving towards lower temperatures and higher injections in Fig. 10, the approximation $k_{BA} \approx 0$ quickly becomes invalid (red region). The origin of this behavior is the onset of temporary recovery which suppresses the LeTID extent by depleting the defect state in favor of the precursor state. The strong gradient in Fig. 9 is thus largely governed by the interplay between temporary recovery and degradation. A quasi-equilibrium between the states A and B forms according to:

$$NDD_{eq}=\frac{A_0 k_{AB}}{k_{AB}+k_{BA}} \quad (14)$$

We have postulated previously that the impact of temporary recovery is the reason why gallium-doped silicon is often seen as inherently LeTID immune [41]. Our kinetic parameters suggest that this temporary recovery induced LeTID suppression can be present at temperatures up to and above 100 °C, depending on the injection. However, a full LeTID resistance in Si:Ga is only observed when low temperatures are combined with a high injection. Since the minority charge carrier density and temperature in a module can range between $10^{14}-10^{15}$cm^{-3} and 60 °C–80 °C, respectively, i.e. to the bottom left of Fig. 9, LeTID defects can appear during field application if precursors exist.

The degradation rate of the full model varies significantly over the whole parameter space even in the regime where the degradation extent plateaus. As Fig. 11 shows, the time required to reach the degradation maximum can be significantly decreased by increasing the temperature and the injection. This effect can be used for rapid testing of the maximum possible LeTID extent, e.g. at 140 °C and 5×10^{15}cm^{-3}. The discontinuities in the contour lines below 80 °C stem from numerical issues in determining the maximum of a curve with a very flat plateau, as obtained when temporary recovery and degradation cause the formation of a quasi-equilibrium.

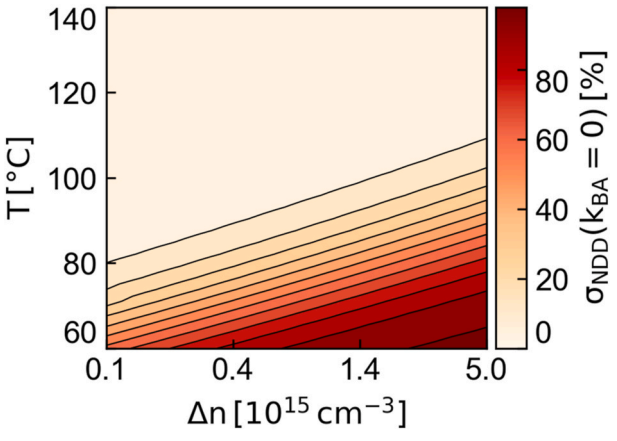

Fig. 10. Deviation in degradation extent between the model neglecting temporary recovery from the complete three-state model as a function of temperature and injection. The deviations become large at the latest below 80 °C, highlighting that temporary recovery is always a dominant process for LeTID in gallium-doped silicon. (For interpretation of the references to color in this figure legend, the reader is referred to the Web version of this article.)

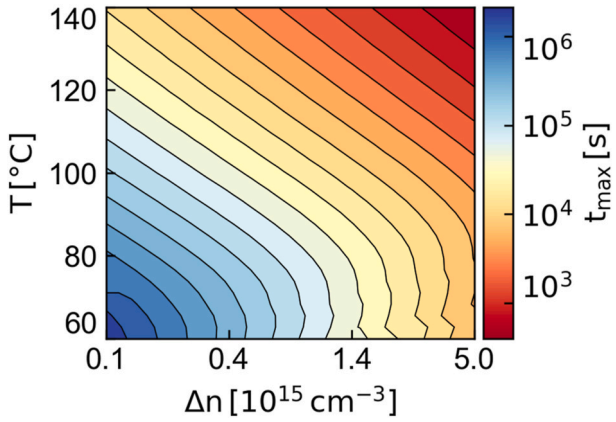

Fig. 11. Time required to reach the maximum degradation extent as a function of temperature and minority charge carrier density.

With the full set of kinetic parameters, it is possible to determine the rate and extent of LeTID in gallium-doped silicon. This is key for top-level models aiming to predict the levelized cost of efficiency of modules depending on climate conditions [56]. Furthermore, the model allows to illustrate which transitions can be neglected in certain ranges of temperature and minority charge carrier density.

5. Conclusions

By investigating temporary recovery in gallium-doped silicon in isolation from degradation and regeneration, we found that the rate of temporary recovery increases as temperature is reduced. This is quantitatively reflected in a reversed Arrhenius behavior with a negative activation energy of $E_a^{BA} = -0.6$ eV. We conclude that temporary recovery is likely a composite process of the type $S \underset{k_1'}{\overset{k_1}{\rightleftarrows}} I \overset{k_2}{\rightarrow} F$ or similar. The reversed Arrhenius behavior imposes certain restrictions ($E_1' > E_1 + E_1$, $k_2 \ll k_1'$ and $A_1' \gg A_1$) on the reaction which could help unraveling its atomic interpretation. The determined injection exponent of $x_{BA} = 1.9$ is in line with previous studies. For degradation and regeneration, the similar activation energies near 0.8 eV suggest that both processes are associated with similar chemical reactions. This is consistent with a model proposed for boron-doped silicon wherein atomic hydrogen binds to a preexisting species for both reactions [21].

By combination with our previous work [41], we have established a complete parametric description of LeTID in gallium-doped silicon. This allows to predict the degradation rate and its extent as a function of temperature and minority charge carrier density. Degradation and regeneration dominate LeTID only for high temperatures above 100 °C. Below that, temporary recovery can significantly suppress the LeTID extent. However, this suppression becomes less pronounced towards lower injections, suggesting that a reduction of precursor concentration is still necessary to completely mitigate LeTID in gallium-doped silicon.

CRediT authorship contribution statement

Fabian T. Thome: Writing – review & editing, Writing – original draft, Visualization, Validation, Methodology, Investigation, Funding

acquisition, Formal analysis, Data curation, Conceptualization. **Elvin Garashli:** Methodology, Investigation. **Wolfram Kwapil:** Writing – review & editing, Supervision, Project administration, Funding acquisition, Conceptualization. **Florian Schindler:** Writing – review & editing, Supervision, Project administration, Funding acquisition. **Martin C. Schubert:** Writing – review & editing, Supervision, Project administration, Funding acquisition, Conceptualization.

Funding sources

The authors acknowledge the financial support by the Federal Ministry for Economic Affairs and Climate Action of Germany in the project GagaRIn (funding codes 03EE1133A and 03EE1133B). The work of Fabian T. Thome was supported by the scholarship of the German Federal Environmental Foundation ("Deutsche Bundesstiftung Umwelt").

Declaration of competing interest

The authors declare that they have no known competing financial interests or personal relationships that could have appeared to influence the work reported in this paper.

Acknowledgements

The tools ChatGPT and DeepL were used for polishing the language and grammar of the self-written manuscript.

Appendix A. Supplementary data

Supplementary data to this article can be found online at https://doi.org/10.1016/j.solmat.2025.113854.

Data availability

Data sets generated during the current study are available from the corresponding author on reasonable request.

References

[1] M. Fischer, M. Woodhouse, T. Brammer, B. Puzant, International Technology Roadmap for Photovoltaic (ITRPV), sixteenth ed., 2025. VDMA e. V., Frankfurt am Main, Germany.
[2] S. Philipps, W. Warmuth, Photovoltaics Report, Fraunhofer ISE and PSE Projects GmbH, 2024. https://www.ise.fraunhofer.de/en/publications/studies/photovoltaics-report.html. (Accessed 5 May 2025).
[3] C. Ballif, F.-J. Haug, M. Boccard, P.J. Verlinden, G. Hahn, Status and perspectives of crystalline silicon photovoltaics in research and industry, Nat. Rev. Mater. 7 (2022) 597–616, https://doi.org/10.1038/s41578-022-00423-2.
[4] S.W. Glunz, B. Steinhauser, J.-I. Polzin, C. Luderer, B. Grübel, T. Niewelt, A.M.O. M. Okasha, M. Bories, H. Nagel, K. Krieg, F. Feldmann, A. Richter, M. Bivour, M. Hermle, Silicon-based passivating contacts: the TOPCon route, Prog. Photovoltaics Res. Appl. 31 (2023) 341–359, https://doi.org/10.1002/pip.3522.
[5] R. Basnet, A. Kashizadeh, C. Mule, W. Han, H. Shen, C. Taylor, S. Agarwal, Y. Wang, P. Stradins, D. Macdonald, Antimony-doped Cz silicon wafers: the next generation of n-type wafers for solar cells?. Conference Presentation Presented at the Silicon PV, 2025.
[6] W. Kwapil, J. Dalke, R. Post, T. Niewelt, Influence of dopant elements on degradation phenomena in B- and Ga-Doped czochralski-grown silicon, Sol. RRL 5 (2021) 2100147, https://doi.org/10.1002/solr.202100147.
[7] K. Ramspeck, S. Zimmermann, H. Nagel, A. Metz, Y. Gassenbauer, B. Birkmann, A. Seidl, Light induced degradation of rear passivated mc-Si solar cells, in: 27th Eur. Photovolt. Sol. Energy Conf., Exhib., WIP, 2012, pp. 861–865, https://doi.org/10.4229/27THEUPVSEC2012-2DO.3.4.
[8] F. Kersten, P. Engelhart, H.-C. Ploigt, A. Stekolnikov, T. Lindner, F. Stenzel, M. Bartzsch, A. Szpeth, K. Petter, J. Heitmann, J.W. Müller, Degradation of multicrystalline silicon solar cells and modules after illumination at elevated temperature, Sol. Energy Mater. Sol. Cells 142 (2015) 83–86, https://doi.org/10.1016/j.solmat.2015.06.015.
[9] D. Bredemeier, D. Walter, J. Schmidt, Light-induced lifetime degradation in high-performance multicrystalline silicon: detailed kinetics of the defect activation, Sol. Energy Mater. Sol. Cells 173 (2017) 2–5, https://doi.org/10.1016/j.solmat.2017.08.007.
[10] W. Kwapil, T. Niewelt, M.C. Schubert, Kinetics of carrier-induced degradation at elevated temperature in multicrystalline silicon solar cells, Sol. Energy Mater. Sol. Cells 173 (2017) 80–84, https://doi.org/10.1016/j.solmat.2017.05.066.
[11] J.M. Fritz, A. Zuschlag, D. Skorka, A. Schmid, G. Hahn, Temperature dependent degradation and regeneration of differently doped mc-Si materials, Energy Proc. 124 (2017) 718–725, https://doi.org/10.1016/j.egypro.2017.09.085.
[12] N.E. Grant, J.R. Scowcroft, A.I. Pointon, M. Al-Amin, P.P. Altermatt, J.D. Murphy, Lifetime instabilities in gallium doped monocrystalline PERC silicon solar cells, Sol. Energy Mater. Sol. Cells 206 (2020) 110299, https://doi.org/10.1016/j.solmat.2019.110299.
[13] D. Lin, Z. Hu, L. Song, D. Yang, X. Yu, Investigation on the light and elevated temperature induced degradation of gallium-doped Cz-Si, Sol. Energy 225 (2021) 407–411, https://doi.org/10.1016/j.solener.2021.07.023.
[14] M. Winter, D.C. Walter, B. Min, R. Peibst, R. Brendel, J. Schmidt, Light and elevated temperature induced degradation and recovery of gallium-doped Czochralski-silicon solar cells, Sci. Rep. 12 (2022) 8089, https://doi.org/10.1038/s41598-022-11831-3.
[15] T. Niewelt, J. Broisch, J. Schön, J. Haunschild, S. Rein, W. Warta, M.C. Schubert, Light-induced degradation and regeneration in n-type silicon, Energy Proc. 77 (2015) 626–632, https://doi.org/10.1016/j.egypro.2015.07.090.
[16] M. Mehler, N. Weinert, N. Aßmann, A. Herguth, G. Hahn, F. Geml, Long-term carrier lifetime instabilities in n-type FZ- and Cz-silicon under illumination at elevated temperature, Sol. Energy Mater. Sol. Cells 278 (2024) 113169, https://doi.org/10.1016/j.solmat.2024.113169.
[17] J. Kamphues, J. Miech, S.M. Warmbold, W. Han, Y. Wang, A. Herguth, G. Hahn, F. Geml, Impact of LeTID in industrial P- and Sb-doped Cz-Si ingots with melt recharging. Conference Presentation Presented at the Silicon PV, 2025.
[18] D. Bredemeier, D. Walter, S. Herlufsen, J. Schmidt, Lifetime degradation and regeneration in multicrystalline silicon under illumination at elevated temperature, AIP Adv. 6 (2016) 035119, https://doi.org/10.1063/1.4944839.
[19] T.H. Fung, M. Kim, D. Chen, C.E. Chan, B.J. Hallam, R. Chen, D.N.R. Payne, A. Ciesla, S.R. Wenham, M.D. Abbott, A four-state kinetic model for the carrier-induced degradation in multicrystalline silicon: introducing the reservoir state, Sol. Energy Mater. Sol. Cells 184 (2018) 48–56, https://doi.org/10.1016/j.solmat.2018.04.024.
[20] A. Herguth, C. Derricks, P. Keller, B. Terheiden, Recovery of LeTID by low intensity illumination: reaction kinetics, completeness and threshold temperature, Energy Proc. 124 (2017) 740–744, https://doi.org/10.1016/j.egypro.2017.09.090.
[21] B. Hammann, F. Schindler, J. Schön, W. Kwapil, M.C. Schubert, S.W. Glunz, Review on hydrogen in silicon solar cells: from its origin to its detrimental effects, Sol. Energy Mater. Sol. Cells 282 (2025) 113432, https://doi.org/10.1016/j.solmat.2025.113432.
[22] B. Hammann, P. Vieira Rodrigues, N. Aßmann, W. Kwapil, F. Schindler, M. C. Schubert, S.W. Glunz, Deciphering the role of hydrogen in the degradation of silicon solar cells under light and elevated temperature, Sol. RRL 8 (2024) 2400457, https://doi.org/10.1002/solr.202400457.
[23] R. Zerfaß, J. Simon, A. Herguth, G. Hahn, Impact of hydrogen in Ga-Doped silicon on maximum LeTID defect density, Sol. RRL (2023) 2300501, https://doi.org/10.1002/solr.202300501.
[24] F. Maischner, S. Maus, J. Greulich, S. Lohmüller, E. Lohmüller, P. Saint-Cast, D. Ourinson, H. Vahlman, K. Hergert, S. Riepe, S. Glunz, S. Rein, LeTID mitigation via an adapted firing process in p-type PERC cells from SMART cast-monocrystalline, czochralski and high-performance multicrystalline silicon, Prog. Photovoltaics Res. Appl. 30 (2022) 123–131, https://doi.org/10.1002/pip.3467.
[25] U. Varshney, M. Kim, M.U. Khan, P. Hamer, C. Chan, M. Abbott, B. Hoex, Impact of substrate thickness on the degradation in multicrystalline silicon, IEEE J. Photovoltaics 11 (2021) 65–72, https://doi.org/10.1109/JPHOTOV.2020.3038412.
[26] R. Eberle, W. Kwapil, F. Schindler, M.C. Schubert, S.W. Glunz, Impact of the firing temperature profile on light induced degradation of multicrystalline silicon, Phys. Status Solidi RRL 10 (2016) 861–865, https://doi.org/10.1002/pssr.201600272.
[27] F. Maischner, W. Kwapil, J.M. Greulich, Y. Jung, H. Höffler, P. Saint-Cast, M. C. Schubert, S. Rein, S.W. Glunz, Process influences on LeTID in Ga-doped silicon, Sol. Energy Mater. Sol. Cells 260 (2023) 112451, https://doi.org/10.1016/j.solmat.2023.112451.
[28] D. Chen, M. Kim, B.V. Stefani, B.J. Hallam, M.D. Abbott, C.E. Chan, R. Chen, D.N. R. Payne, N. Nampalli, A. Ciesla, T.H. Fung, K. Kim, S.R. Wenham, Evidence of an identical firing-activated carrier-induced defect in monocrystalline and multicrystalline silicon, Sol. Energy Mater. Sol. Cells 172 (2017) 293–300, https://doi.org/10.1016/j.solmat.2017.08.003.
[29] F. Maischner, J.M. Greulich, W. Kwapil, D. Ourinson, S.W. Glunz, S. Rein, LeTID mitigation via an adapted firing process in p-type PERC cells from gallium-doped czochralski silicon, Sol. Energy Mater. Sol. Cells 262 (2023) 112529, https://doi.org/10.1016/j.solmat.2023.112529.
[30] B. Hammann, N. Aßmann, J. Schön, W. Kwapil, F. Schindler, S. Roder, E. V. Monakhov, M.C. Schubert, Understanding the impact of the cooling ramp of the fast-firing process on light- and elevated-temperature-induced degradation, Sol. Energy Mater. Sol. Cells 259 (2023) 112462, https://doi.org/10.1016/j.solmat.2023.112462.
[31] M. Winter, D.C. Walter, J. Schmidt, Impact of fast-firing conditions on Light- and elevated-temperature-induced degradation (LeTID) in Ga-Doped Cz–Si, IEEE J. Photovoltaics (2023) 1–9, https://doi.org/10.1109/JPHOTOV.2023.3304118.
[32] D. Bredemeier, D.C. Walter, J. Schmidt, Possible candidates for impurities in mc-Si wafers responsible for light-induced lifetime degradation and regeneration, Sol. RRL 2 (2018) 1700159, https://doi.org/10.1002/solr.201700159.

[33] U. Varshney, M. Abbott, A. Ciesla, D. Chen, S. Liu, C. Sen, M. Kim, S. Wenham, B. Hoex, C. Chan, Evaluating the impact of SiN_x thickness on lifetime degradation in silicon, IEEE J. Photovoltaics 9 (2019) 601–607, https://doi.org/10.1109/JPHOTOV.2019.2896671.

[34] D. Bredemeier, D.C. Walter, R. Heller, J. Schmidt, Impact of hydrogen-rich silicon nitride material properties on light-induced lifetime degradation in multicrystalline silicon, Phys. Status Solidi RRL 13 (2019) 1900201, https://doi.org/10.1002/pssr.201900201.

[35] L. Helmich, D.C. Walter, D. Bredemeier, J. Schmidt, Atomic-layer-deposited Al_2O_3 as effective barrier against the diffusion of hydrogen from sinx:h layers into crystalline silicon during rapid thermal annealing, Phys. Status Solidi RRL 14 (2020) 2000367, https://doi.org/10.1002/pssr.202000367.

[36] U. Varshney, B. Hallam, P. Hamer, A. Ciesla, D. Chen, S. Liu, C. Sen, A. Samadi, M. Abbott, C. Chan, B. Hoex, Controlling Light- and elevated-temperature-induced degradation with thin film barrier layers, IEEE J. Photovoltaics 10 (2020) 19–27, https://doi.org/10.1109/JPHOTOV.2019.2945199.

[37] A. Schmid, C. Fischer, D. Skorka, A. Herguth, C. Winter, A. Zuschlag, G. Hahn, On the role of AlO_x thickness in AlO_x/SiN_y:H layer stacks regarding Light- and elevated temperature-induced degradation and hydrogen diffusion in c-Si, IEEE J. Photovoltaics 11 (2021) 967–973, https://doi.org/10.1109/JPHOTOV.2021.3075850.

[38] W. Kwapil, J. Schön, T. Niewelt, M.C. Schubert, Temporary recovery of the defect responsible for Light- and elevated temperature-induced degradation: insights into the physical mechanisms behind LeTID, IEEE J. Photovoltaics 10 (2020) 1591–1603, https://doi.org/10.1109/JPHOTOV.2020.3025240.

[39] Gallium-Doped Monocrystalline Silicon Fully Solves the Problem of a PERC Module's LID, LONGi News, 2020. https://www.longi.com/en/news/6880/. (Accessed 29 January 2024).

[40] M. Winter, D. Walter, J. Schmidt, Carrier lifetime degradation and regeneration in Gallium- and boron-doped monocrystalline silicon materials, IEEE J. Photovoltaics 11 (2021) 866–872, https://doi.org/10.1109/JPHOTOV.2021.3070474.

[41] F.T. Thome, C. Yilmaz, W. Kwapil, F. Schindler, M.C. Schubert, Why is gallium-doped silicon (sometimes) stable? Kinetics of light and elevated temperature induced degradation, Sol. Energy Mater. Sol. Cells 275 (2024) 112986, https://doi.org/10.1016/j.solmat.2024.112986.

[42] F.T. Thome, P. Meßmer, S. Mack, E. Schnabel, F. Schindler, W. Kwapil, M. C. Schubert, UV-Induced degradation of industrial PERC, TOPCon, and HJT solar cells: the next big reliability challenge? Sol. RRL 8 (2024) 2400628 https://doi.org/10.1002/solr.202400628.

[43] T. Niewelt, F. Maischner, W. Kwapil, E. Khorani, S.L. Pain, Y. Jung, E.C.B. Hopkins, M. Frosch, P.P. Altermatt, H. Guo, Y.C. Wang, N.E. Grant, J.D. Murphy, Stability of industrial gallium-doped czochralski silicon PERC cells and wafers, Sol. Energy Mater. Sol. Cells 266 (2024) 112645, https://doi.org/10.1016/j.solmat.2023.112645.

[44] H. Höffler, F. Schindler, A. Brand, D. Herrmann, R. Eberle, R. Post, A. Kessel, J. Greulich, M.C. Schubert, Review and recent development in combining photoluminescence-and electroluminescence-imaging with carrier lifetime measurements via modulated photoluminescence at variable temperatures, in: Proc. 37th Eur. PV Sol. Energy Conf, Exhib., 2020.

[45] J.A. Giesecke, M.C. Schubert, B. Michl, F. Schindler, W. Warta, Minority carrier lifetime imaging of silicon wafers calibrated by quasi-steady-state photoluminescence, Sol. Energy Mater. Sol. Cells 95 (2011) 1011–1018, https://doi.org/10.1016/j.solmat.2010.12.016.

[46] T. Trupke, R.A. Bardos, M.D. Abbott, Self-consistent calibration of photoluminescence and photoconductance lifetime measurements, Appl. Phys. Lett. 87 (2005) 184102, https://doi.org/10.1063/1.2119411.

[47] J.A. Giesecke, M.C. Schubert, D. Walter, W. Warta, Minority carrier lifetime in silicon wafers from quasi-steady-state photoluminescence, Appl. Phys. Lett. 97 (2010) 092109, https://doi.org/10.1063/1.3485216.

[48] J.A. Giesecke, M.C. Schubert, W. Warta, Self-sufficient minority carrier lifetime in silicon from quasi-steady-state photoluminescence, Phys. Status Solidi A 209 (2012) 2286–2290, https://doi.org/10.1002/pssa.201228383.

[49] S. Joos, A. Herguth, U. Hess, J. Ebser, S. Seren, B. Terheiden, G. Hahn, Light induced curing (LIC) of passivation layers deposited on native silicon oxide, Energy Proc. 27 (2012) 349–354, https://doi.org/10.1016/j.egypro.2012.07.075.

[50] J. Horzel, S. Mack, I. Voicu Vulcanean, K. Zimmermann, S. Pingel, W. Kwapil, F. Maischner, H. Höffler, S. Bashardoust, D. Wagenmann, J. Greulich, J. Seif, A. Steinmetz, J. Rentsch, High lifetime Ga-Doped Cz-Si for carrier-selective junction solar cells, Sol. RRL (2023) 2200613, https://doi.org/10.1002/solr.202200613.

[51] T.U. Nærland, S. Bernardini, H. Haug, S. Grini, L. Vines, N. Stoddard, M. Bertoni, On the recombination centers of iron-gallium pairs in Ga-doped silicon, J. Appl. Phys. 122 (2017) 085703, https://doi.org/10.1063/1.5000358.

[52] N.M. Johnson, C. Herring, Kinetics of minority-carrier-enhanced Dissociation of hydrogen-dopant Complexes in Semiconductors, 1992, p. 4.

[53] F. Kersten, F. Fertig, K. Petter, B. Klöter, E. Herzog, M.B. Strobel, J. Heitmann, J. W. Müller, System performance loss due to LeTID, Energy Proc. 124 (2017) 540–546, https://doi.org/10.1016/j.egypro.2017.09.260.

[54] E. Fokuhl, D. Philipp, G. Mülhöfer, P. Gebhardt, LID and LETID evolution of PV modules during outdoor operation and indoor tests, EPJ Photovolt 12 (2021) 9, https://doi.org/10.1051/epjpv/2021009.

[55] M.G. Deceglie, T.J. Silverman, S.W. Johnston, J.A. Rand, M.J. Reed, R. Flottemesch, I.L. Repins, Light and elevated temperature induced degradation (LeTID) in a utility-scale photovoltaic system, IEEE J. Photovoltaics 10 (2020) 1084–1092, https://doi.org/10.1109/JPHOTOV.2020.2989168.

[56] I.L. Repins, D.C. Jordan, M. Woodhouse, M. Theristis, J.S. Stein, H.P. Seigneur, D. J. Colvin, J.F. Karas, A.N. McPherson, C. Deline, Long-term impact of light- and elevated temperature-induced degradation on photovoltaic arrays, MRS Bull. 48 (2023) 589–601, https://doi.org/10.1557/s43577-022-00438-8.

[57] P. Atkins, J. De Paula, The rates of chemical reactions, in: Phys. Chem., ninth ed., Oxford University Press, New York, 2010, p. 811.

[58] A. Menon, N. Sathyamurthy, Negative activation energy for the Cl(Br)O + NO → Cl (Br) + NO_2 reactions, J. Phys. Chem. 85 (1981) 1021–1023.

[59] M. Mozurkewich, S.W. Benson, Negative activation energies and curved arrhenius plots. 1. Theory of reactions over potential well, J. Phys. Chem. 88 (1984) 6429–6435.

[60] M. Mozurkewich, S.W. Benson, Negative activation energies and curved arrhenius plots. 2. OH + CO, J. Phys. Chem. 88 (1984) 6435–6441.

[61] L.E. Revell, G.E. Bodeker, D. Smale, R. Lehmann, P.E. Huck, B.E. Williamson, E. Rozanov, H. Struthers, The effectiveness of N_2O in depleting stratospheric ozone, Geophys. Res. Lett. 39 (2012), https://doi.org/10.1029/2012GL052143.

[62] L.E. Revell, B.E. Williamson, Why are some reactions slower at higher temperatures? J. Chem. Educ. 90 (2013) 1024–1027, https://doi.org/10.1021/ed400086w.